Three-Channel Transmission Line Impedance Model for Mesoscopic Oxide Electrodes Functionalized with a Conductive Coating

Juan Bisquert,*,† Michael Grätzel,*,‡ Qing Wang,‡ and Francisco Fabregat-Santiago†

Departament de Ciències Experimentals, Universitat Jaume I, 12071 Castelló, Spain, and Laboratory for Photonics and Interfaces, Institute of Chemical Sciences and Engineering, Swiss Federal Institute of Technology, CH-1015 Lausanne, Switzerland

Received: February 23, 2006; In Final Form: March 28, 2006

A three-channel transmission line (TL) impedance model is proposed to address the charge transport behavior of molecular functionalized mesoscopic oxide electrodes at different bias conditions. A full general solution of the three-channel TL for the system is provided in this paper. Selected experimental results of impedance spectroscopy of mesoscopic Al_2O_3 and TiO_2 networks, covered with a monolayer of Ru complex *cis*-RuLL′-$(NCS)_2$ (L = 2,2′-bipyridyl-4,4′-dicarboxylic acid, L′ = 4,4′-dinonyl-2,2′-bipyridyl) (Z907), are briefly discussed. It shows that the model constitutes a useful tool for characterizing nanoporous electrodes functionalized with organic conducting layers in the surface. The model makes it possible to determine the separate conductivity of substrate oxide and molecular layer, and interfacial charge transfer, in the functionalized nanostructured electrodes.

1. Introduction

Transmission line (TL) equivalent circuits are widely used for representing impedance spectroscopy models in electrochemistry and related areas. Two basic kinds of TL models for electroactive electrodes can be distinguished. The first kind is for transport of one or more species in a homogeneous medium. For example, diffusion of a single species is described with a two-channel transmission line, with resistors in one channel accounting for the conductivity and capacitances in the transverse branches corresponding to the chemical capacitance.[1−4] Eventually, the transverse branch of the TL contains a recombination or reaction resistance that describes the loss of the diffusing species.[1,4] For two oppositely charged species, the classical solution with local electroneutrality gives a three-channel transmission line where the central channel contains a chain of capacitors that describes the local polarization.[5] This last model is used for ionic transport of a dissociated salt in a membrane[5] and also for the transport of electronic species in semiconductors[6−8] and electronically conducting polymers.[9,10]

The second class of models applies in a heterogeneous structure with several spatially mixed phases, each of which is separately continuously connected, as in porous electrodes.[11−15] This class of models, as well as the former one, takes a macrohomogeneous approach that derives the generalized equivalent circuit elements by using average properties.[12] Indeed, in the porous electrode models, the different channels and transverse elements in the TL do not represent individual structural units, but, respectively, the carrier transport along the separate phases in the system and the possible transference of carriers and polarization between the phases.[12] Most models of this kind are two-channel transmission lines, one channel for the solid porous structure and another one for the electrolyte filling the pores.[11−15] This standard two-channel TL is represented in Figure 1. The meaning of this equivalent circuit is discussed, for example, in ref 14, and it is especially useful for investigating electrochemical systems with phases of strongly varying conductivity depending on the bias potential.[16]

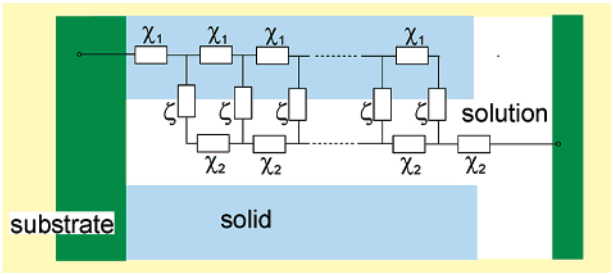

Figure 1. Scheme of the two-channel transmission line model for a porous electrode in electrolyte solution. χ_1 is the specific conductivity in the solid phase, χ_2 is the specific conductivity in the liquid electrolyte, and ζ is the specific polarization/charge-transfer element at the solid/liquid interface.

Molecular functionalized mesoscopic oxide electrodes have been widely investigated in recent years for applications in dye-sensitized solar cells[17] and other electrooptical devices such as electrochromic windows.[18] In these systems, the solid structure is composed of an array of sintered colloidal semiconductor nanoparticles that is covered with a monolayer of dye molecules, and the functionalized electrode is immersed in electrolyte solution, as indicated in Figure 2a. Usually, in these systems, the electronic communication between the large internal surface covered with optically active molecules and the external contact occurs by electron transport through the assembly of sintered semiconductor nanoparticles. Impedance spectroscopy has proved to be a very useful technique for the characterization of properties of dye solar cells[1,19−22] and electrochromic windows.[23]

Recently, a new approach has been taken[24−28] toward electric and electrooptic devices formed by molecular functionalized mesoscopic oxides, such as photovoltaic cells, sensors, and

* Corresponding authors. E-mail: bisquert@uji.es (J.B.); michael.graetzel@epfl.ch (M.G.).
† Departament de Ciències Experimentals, Universitat Jaume I.
‡ Laboratory for Photonics and Interfaces, Institute of Chemical Sciences and Engineering, Swiss Federal Institute of Technology.

10.1021/jp0611727 CCC: $33.50
Published on Web 05/18/2006

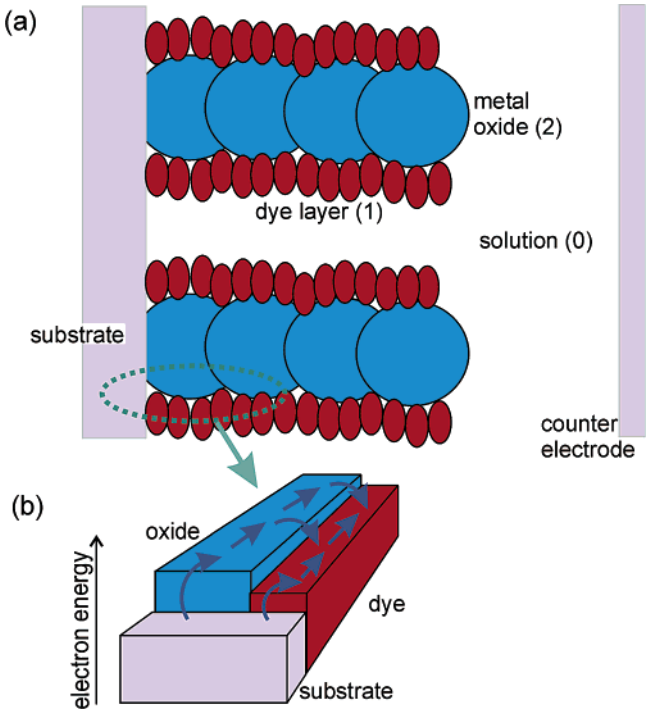

Figure 2. (a) Scheme of a nanostructured electrode composed of sintered metal oxide nanoparticles, covered with a layer of organic dye molecules, and immersed in conducting solution. (b) Schematic energy picture of the injection of electrons from the substrate to the oxide and dye phases, and the consequent electron transport and transfer between these last two phases. The electron flow direction is suggested by arrows, but the electrochemical potentials (quasi-Fermi levels) determining the directions of electron flow are not indicated explicitelly.

switchable molecular electronics, etc., in which the molecular layer adsorbed in the surface serves, instead or in addition to the optical functions commented above, as an electron or hole transport relay. It was shown that the molecular layer can be charged either with electrons or holes from the substrate, depending on the applied bias potential.[25,26] There are, therefore, three possible paths, normal to the macroscopic contacts, for electronic species in this system: the semiconductor nanostructure, the molecular layer, and the solution (with a redox carrier). The first two are connected to the conducting substrate, as indicated in Figure 2b, while the third one is connected to the counterelectrode.

Because there are several ways to electronically address the solid network in these systems, a rich behavior of electron transport and charge-transfer properties is expected. The case suggested as an example in Figure 2b consists of organic molecules in which the energy of the lowest unoccupied molecular orbital (LUMO) is similar or lower than the lower edge of the semiconductor conduction band. In this situation, the organic layer can be electron charged, either from the semiconductor nanostructure[23] or from the substrate, or with a combination of both, depending on the conductivity of the two phases and the charge-transfer kinetics. Very recently, heteroleptic Ru complexes for dye-sensitized solar cells, such as the hydrophobic Z907 dye molecule, have been found to show such behavior on mesoscopic oxide films,[26] where good spatial overlap of adjacent molecular orbitals forms a macroscopic conduction pathway and across surface charge transfer can take place through either the overlapping HOMOs (hole) or LUMOs (electrons). As illustrated in Figure 3, in a TiO_2 mesoscopic network, covered with a monolayer of Z907 dye, carrier

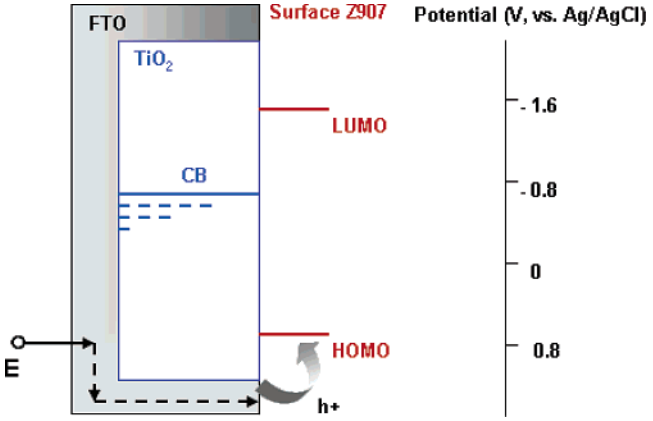

Figure 3. Energy level of Z907-derivatized mesoscopic TiO2 film. The dashed lines show the surface states distributed below the conduction band (CB) of TiO2. When the FTO substrate is polarized to 0.8 V, holes flow through the conducting substrate and inject into the HOMO of adjacent Z907 molecules, as indicated by the arrows. The right axis shows the relative potential vs Ag/AgCl.

transport at negative bias should occur primarily through TiO_2 network, while at positive bias potential, it will take place by hole conduction through the molecular layer.[26] And, of course, if the mesoscopic oxide layer is insulating, as in the case of colloidal Al_2O_3 networks, then conduction at the surface molecular layer will prevail both at positive and negative potential bias.[25,26]

Impedance spectroscopy appears as a useful tool to investigate the detailed and varied properties of the mesoscopic oxide electrodes functionalized with molecular-conducting layers. However, one must consider the aspect that makes this system different from the classical porous electrode model. Figure 2b shows that the standard "solid" pathway of the two-channel transmission line, shown in Figure 1, is split into two parallel pathways intimately connected with charge-transfer events. For materials with strongly varying conduction and charge transfer as function of the external bias, as those forming molecular-conducting functionalized mesoscopic oxide electrodes, one cannot a priori determine which should be the primary paths for electron transport in the oxide/dye combination. Therefore, a general analysis of impedance spectroscopy of these systems, able to discriminate electron transport in oxide and molecular layer, requires a TL model of at least *three* transport channels, corresponding to the three conducting phases, two of which have variable resistivity, with the possibility of charge-transfer between the separate phases.

To our knowledge, there are no solutions of three-channel transmission lines for porous electrodes in the literature. In this paper, we provide a full general solution of the three-channel TL for the system of Figure 2, and we discuss some interesting particular realizations of the TL. Selected experimental results of impedance spectroscopy of colloidal Al_2O_3 and TiO_2 networks, covered with a monolayer of Z907, as shown in Figure 3, are briefly discussed. We, therefore, show that the model constitutes a useful tool for characterizing nanoporous electrodes functionalized with organic conducting layers in the surface.

2. Experimental Section

A paste consisting of 20-nm TiO_2 or 6-nm Al_2O_3 colloid and ethyl cellulose in terpineol was deposited using the doctor blade

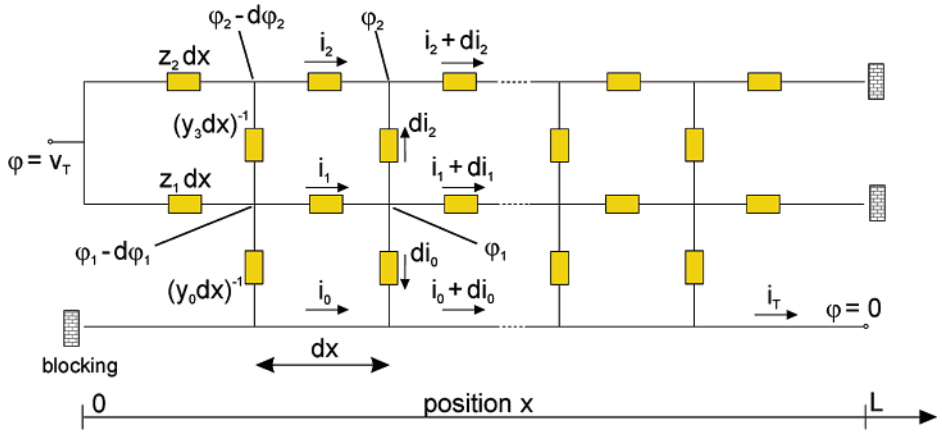

Figure 4. Scheme of the three-channel transmission line model for the system of Figure 2a. The meaning of the different elements is indicated in the main text.

technique on a fluorine-doped SnO_2 (FTO) conducting glass (TEC15, 15 Ω/cm) to form a transparent layer. Subsequently, the deposited film was heated to 500 °C in an oxygen atmosphere and calcined for 10 min. The final film thickness was determined by using an Alpha-Step 200 surface profilometer (Tencor Instruments, USA) to be ca. 5 μm for TiO_2 and 8 μm for Al_2O_3 films. The mesoscopic metal oxide films were first sintered at 500 °C for 20 min in air and after cooling to 80 °C, immersed overnight in a solution of 0.30 mM Ru complex *cis*-RuLL′(NCS)$_2$ (L = 2,2′-bipyridyl-4,4′-dicarboxylic acid, L′ = 4,4′-dinonyl-2,2′-bipyridyl) in a mixture of acetonitrile and *tert*-butyl alcohol (volume ratio, 1:1).

Impedance analysis was performed with a computer-controlled potentiostat (EG&G, M273) equipped with a frequency response analyzer (EG&G, M1025). The frequency range is 0.01−100 kHz. The amplitude of the alternating signal is 5 mV. The electrolyte is 0.1 M $TBAPF_6$ in acetonitrile. Both films were immersed in a 0.1 M $TBAPF_6$/acetonitrile electrolyte. In all cases, a platinum coil and Ag/AgCl electrode were employed as the counter and reference electrode, respectively. Before each measurement, the electrodes were equilibrated for 150 s.

3. Theory

The three-channel TL discussed in this work is shown in Figure 4. Channel 0 is for the electrolyte solution, channel 1 is for the molecular layer, and channel 2 for the metal oxide structure. These last two channels are connected to the conducting substrate, at $x = 0$, and are blocked at the right boundary of the film, at $x = L$, while channel 0 is connected to the right electrode and is blocked at the substrate.

In general, transport and charge-transfer processes in electrochemistry are described by highly nonlinear relations between the driving force (gradient or difference of electrochemical potentials) and particle flux. However, impedance spectroscopy uses a small perturbation over a steady state, hence all relations between difference of electrochemical potential and particle flux are *linear*, the coefficient being a local impedance, and this is why the model may be represented as an equivalent circuit. We denote φ_k, the small perturbation of the electrochemical potential (in units of electrical potential) in channel k, and i_k, the small perturbation of electrical current in channel k. The impedance model is formulated with a set of linear relationships between φ_k and i_k. There are two kinds of such relationships. One kind describes variation of φ_k with *position* in relation to current i_k, in a single channel. We call such a coefficient z_k, and it is related to the driving force for transport, so its archetypal form is a resistance (although more complex forms exist, associated to anomalous transport[29]). Channel 0 is assumed to have a large conductivity, hence there is no longitudinal impedance in this channel.

The other kind of relationship stands for a loss of current in one channel with gain in another one in relation to the local difference of electrochemical potential between the phases. We describe this kind of process with local admittances y. The archetype element is an RC circuit if there is charge transfer between the phases or just capacitance if there is no Faradaic current permitted.

The elements z, distributed in the spatial direction of each channel, are continuously interrupted by interphase elements y. This combination, that corresponds to the physical current flow as suggested in Figure 2b, gives rise to the characteristic structure of a TL. Generally, linear equations for physical quantities varying in space with local dissipation are represented with TLs, for example, acoustic waves.[30]

In the model of Figure 2, considering a slab of thickness dx parallel to the macroscopic contact, we have the following impedances: 0 along channel 0, z_1 dx along channel 1, z_2 dx along channel 2, $(y_0\ \mathrm{d}x)^{-1}$ between channel 0 and 1, and $(y_3\ \mathrm{d}x)^{-1}$ between channel 1 and 2.

Because the total current is conserved, we furthermore have

$$i_T = i_0 + i_1 + i_2 = \text{constant} \qquad (1)$$

This TL model is perhaps the simplest one, considering the three phases involved in Figure 2. Even so, the analytical solution is a quite involved expression, as shown below. More general models with additional connections in the TL could be considered if the metal oxide admits also ions from solution (by intercalation) or loses electrons by charge transfer to solution. One should then extend the model with a connection between phases 0 and 2, but the problem becomes much more severe to solve. We believe that the model presented here should be a good first approximation for impedance spectroscopy of the functionalized nanoporous electrode of Figure 2, including these cases.

From Figure 4 and eq 1, we obtain the system of equations

$$\frac{d\varphi_1}{dx} = -z_1 i_1 \tag{2}$$

$$\frac{d\varphi_2}{dx} = -z_2 i_2 \tag{3}$$

$$\frac{di_1}{dx} = y_3(\varphi_1 - \varphi_2) \tag{4}$$

$$\frac{di_1}{dx} + \frac{di_2}{dx} = y_0 \varphi_1 \tag{5}$$

$\upsilon_T = \varphi(0) - \varphi(L)$ is the (total) ac applied potential, and we take for convenience $\varphi(L) = \varphi_L = 0$. The boundary conditions for potentials of the system of differential equations are:

$$\varphi_{10} = \varphi_{20} = \upsilon_T \tag{6}$$

Boundary conditions on currents correspond to the blocking ends indicated in Figure 4:

$$i_{00} = 0 \tag{7}$$

$$i_{1L} = i_{2L} = 0 \tag{8}$$

In eqs 6−8, the second subscript indicates the point $x = 0$, L. The impedance of the TL is defined as

$$Z = \frac{\upsilon_T}{i_T} \tag{9}$$

The calculation of Z assumes a spatially homogeneous model in which the local impedances are independent of position. For later reference, we introduce the following definitions

$$q^2 = -y_0 y_3 z_1 z_2 \tag{10}$$

$$p = \frac{1}{2}[y_0 z_1 + y_3(z_1 + z_2)] \tag{11}$$

$$b = (q^2 + p^2)^{1/2} \tag{12}$$

$$\alpha = (p + b)^{1/2} \tag{13}$$

$$\beta = (p - b)^{1/2} \tag{14}$$

$$A = \frac{1}{\alpha}\sinh(\alpha L) - \frac{1}{\beta}\sinh(\beta L) \tag{15}$$

$$B = \cosh(\alpha L) - \cosh(\beta L) \tag{16}$$

$$C = \alpha \sinh(\alpha L) - \beta \sinh(\beta L) \tag{17}$$

$$D = \alpha^2 \cosh(\alpha L) - \beta^2 \cosh(\beta L) \tag{18}$$

We make the Laplace transform of the system of eqs 2−5, with the rules $x \rightarrow u$, $\varphi \rightarrow \Phi$, $i \rightarrow I$. We obtain the linear system

$$\begin{bmatrix} u & 0 & z_1 & 0 \\ 0 & u & 0 & z_2 \\ y_3 & -y_3 & 0 & -u \\ y_0 & 0 & u & u \end{bmatrix} \begin{bmatrix} \Phi_1 \\ \Phi_2 \\ I_1 \\ I_2 \end{bmatrix} = \begin{bmatrix} \upsilon_T \\ \upsilon_T \\ -i_{20} \\ i_{10} + i_{20} \end{bmatrix} \tag{19}$$

The solution for the currents is

$$I_1 = \frac{1}{\Delta}[i_{10}u^3 - \upsilon_T y_0 u^2 - (i_{10} + i_{20})y_3 z_2 u + y_0 y_3 z_2 \upsilon_T] \tag{20}$$

$$I_2 = \frac{1}{\Delta}[i_{20}u^3 - i_{20} y_0 z_1 u - (i_{10} + i_{20})y_3 z_1 u + y_0 y_3 z_1 \upsilon_T] \tag{21}$$

$$\Delta = u^4 - 2pu^2 - q^2 \tag{22}$$

We compute the inverse Laplace transform at $x = L$ of the following quantities that appear in eqs 20 and 21:

$$\frac{1}{\Delta} \rightarrow 4bA \tag{23}$$

$$\frac{u}{\Delta} \rightarrow 4bB \tag{24}$$

$$\frac{u^2}{\Delta} \rightarrow 4bC \tag{25}$$

$$\frac{u^3}{\Delta} \rightarrow 4bD \tag{26}$$

With these transformations, we can calculate the currents i_{kL}. Equation 8 gives us two equations from which eq 9 can be calculated with the result

$$Z = y_0^{-1}\frac{D^2 - 2pBD - q^2B^2}{CD - BCy_0 z_1 - ADy_3(z_1 + z_2) - q^2AB} \tag{27}$$

4. Models

Equation 27 stands as the general solution of the TL of Figure 4. For the analysis of specific systems, it is necessary to select the form of the local impedances. Several relevant examples are discussed in the following.

A limiting case of eq 27 is $z_1 = z_2 = 0$, which gives $Z = y_0^{-1}$. The two upper transport channels become shorted, and then current entering from the left contact goes through the middle channel toward the lowest one.

A simple model is shown in Figure 5 (case $\gamma_0 = 1$) in which the transport channels are resistances and transverse impedances are capacitive:

$$z_1 = r_1 = R_1/L \tag{28}$$

$$z_2 = r_2 = R_2/L \tag{29}$$

$$y_0 = j\omega c_0; \qquad c_0 = C_0/L \tag{30}$$

$$y_3 = j\omega c_3; \qquad c_3 = C_3/L \tag{31}$$

Here, ω is the angular frequency and $j = \sqrt{-1}$. Lowercase letters indicate resistance or capacitance per unit length, and uppercase letters correspond to the value of the element for the whole film thickness, L. All calculations assume an electrode of unit area.

In the example shown in the spectrum of Figure 5 for $\gamma_0 = 1$, the resistance is very large in the upper channel, hence the current flows through the central channel and the transverse admittance y_3 is irrelevant. The resistance r_1 coupled with the capacitance c_0 provides the standard impedance behavior[14] of a porous electrode with capacitive interface and infinite conductivity in the electrolyte (Figure 1): a 45° line at high frequency, and the capacitive vertical line at low frequency.

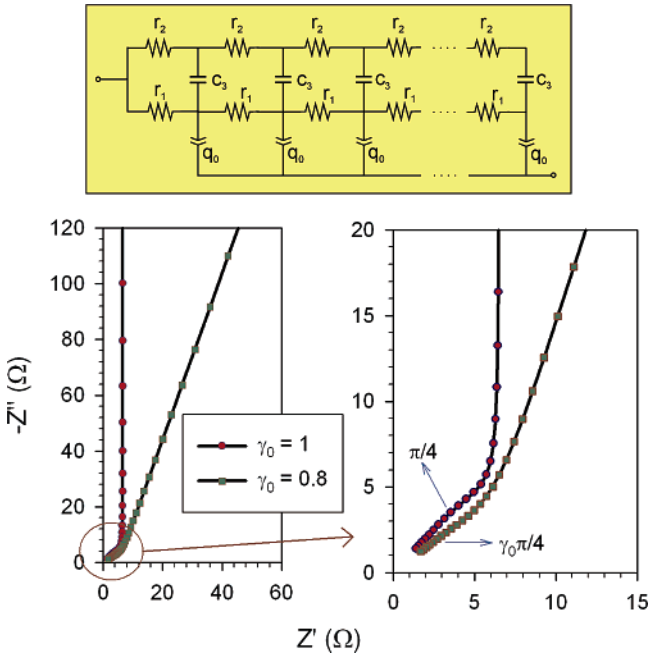

Figure 5. Simulation of the impedance spectra for the transmission line model indicated in the scheme with $R_1 = 20\ \Omega$, $R_2 = 1000\ \Omega$, $Q_0 = 5$ mF $s^{1-\gamma_0}$, $C_3 = 5$ mF and two values of γ_0 as shown. Also indicated is the inclination of the high-frequency line, in radians.

The capacitive response in many real systems does not show a perfect capacitor and is better described by a constant phase element (CPE),[31,32] with admittance

$$y_0 = q_0(j\omega)^{\gamma_0}; \qquad q_0 = Q_0/L \tag{32}$$

Equation 30 is obtained from eq 32 in the particular case $\gamma_0 = 1$. In general, the CPE changes the slopes of the Warburg and/or capacitive lines of the impedance spectra, depending on the extent that the exponent γ departs from the value of 1 of the ideal capacitor. In the example of Figure 5 for $\gamma_0 = 0.8$, the deviations from the ideal model in the low- and high-frequency lines have a common origin in the dispersive element Q_0, hence the slopes are related by the high-frequency line having an exponent $\gamma_0/2$, while the low-frequency line is the full CPE. Hence the latter exponent doubles the former one, as discussed in ref 14.

If instead of the case of the previous example, the resistance is lower in the upper branch of the TL, then the current is forced through the transverse element y_3. Several examples are shown in Figure 6 for a model with charge transfer between channel 1 and 2:

$$y_3 = \frac{1}{r_3} + j\omega c_3; \qquad r_3 = LR_3 \tag{33}$$

At high frequency, c_3 is shunted, and the impedance gives again the standard behavior of the two-channel transmission line shown in Figure 5. But as the frequency decreases, there begins to form an arc due to y_3. At very low frequencies, the impedance is capacitive.

In the next realization of the TL, Figure 7, we have included the effect of charge transfer between channel 1 and the solution (lower channel). Also, capacitances are described by constant phase element (CPE), eq 32, and

$$y_3 = \frac{1}{r_3} + q_3(j\omega)^{\gamma_3}; \qquad q_3 = Q_3/L \tag{34}$$

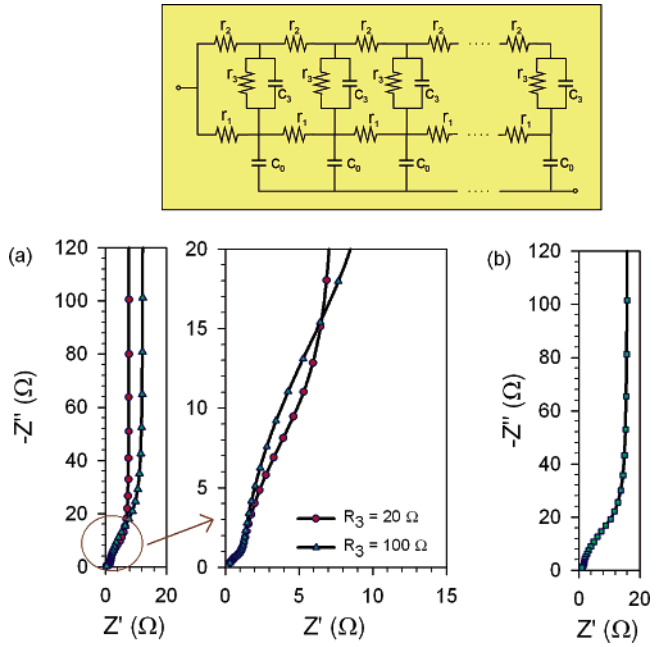

Figure 6. Simulation of the impedance spectra for the transmission line model indicated in the scheme with $C_0 = 5$ mF, $C_3 = 5$ mF, $R_2 = 5\ \Omega$. (a) $R_1 = 40\ \Omega$, (b) $R_1 = 120\ \Omega$, $R_3 = 20\ \Omega$.

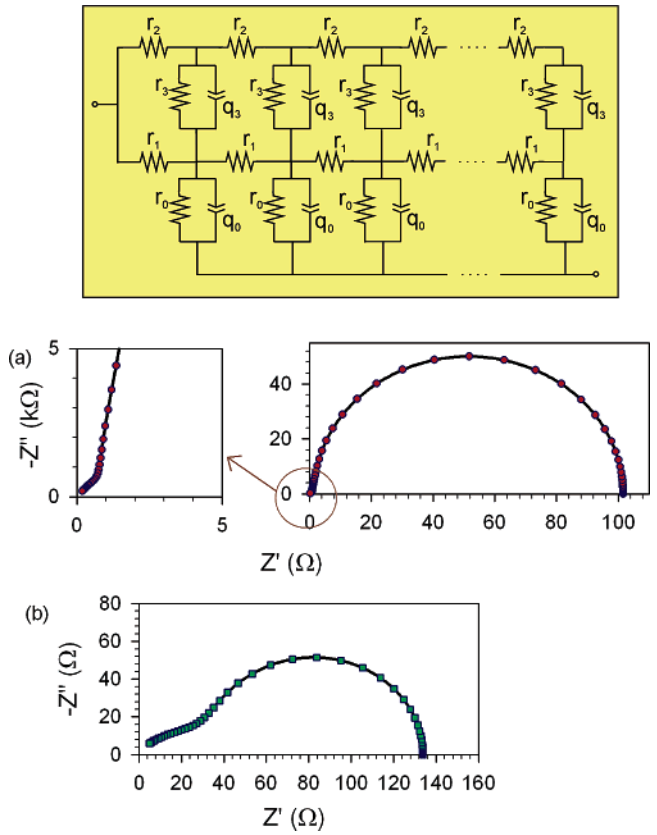

Figure 7. Simulation of the impedance spectra for the transmission line model indicated in the scheme with $R_2 = 5\ \Omega$, $R_0 = 100\ \Omega$, $R_3 = 50\ \Omega$, $Q_0 = 5$ mF $s^{0.2}$, $\gamma_0 = 0.8$, $\gamma_3 = 0.8$. (a) $R_1 = 5\ \Omega$, $Q_3 = 5$ mF $s^{0.2}$, (b) $R_1 = 500\ \Omega$, $Q_3 = 0.05$ mF $s^{0.2}$,

If $R_1 \approx R_2$ (Figure 7a), the current goes through channel 1, and we obtain again the 45° line at high frequency, due to r_1 and q_0, and the reaction arc at low frequency, which is due only to y_0. But if $R_1 \gg R_2$ (Figure 7b), the current enters through channel 2, at least at low frequencies. Then we obtain two

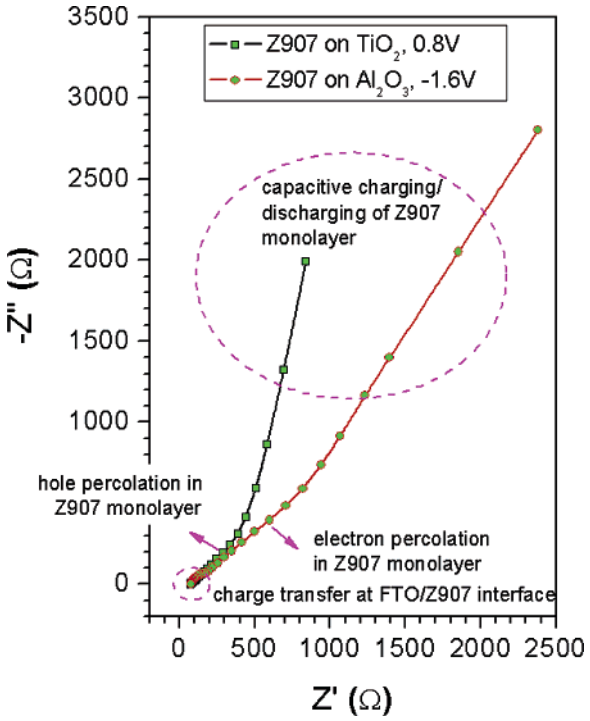

Figure 8. Experimental impedance plots of Z907 derivatized mesoscopic TiO_2 at 0.8 V and Al_2O_3 at −1.6 V. Transport, of holes for TiO_2 and of electrons for Al_2O_3, takes place through Z907 monolayer as its substrate is insulating. The insets show the individual processes occurred at different frequency regions.

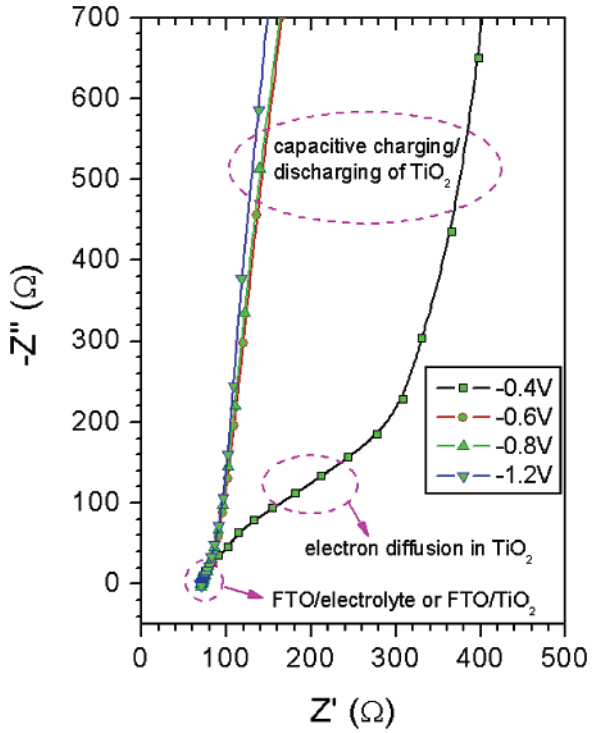

Figure 9. Experimental impedance plots of Z907 derivatized mesoscopic TiO_2 measured at −0.4, −0.6, −0.8, and −1.2 V, where electrons are transported through TiO_2. The insets show the individual processes occurred at different frequency regions.

consecutive arcs due to y_3 and y_0. At very high frequency, the arc turns into the 45° line characteristic of TL behavior.

5. Results and Discussion

In agreement with the theory described above, we present here the impedance data obtained for a film of mesoscopic Al_2O_3, made from 6-nm colloids, covered with a monolayer of Z907, and another one of nanoporous TiO_2, from 20-nm particles, also covered with the same monolayer.

The Al_2O_3 film is completely insulating within the electrochemical window of the electrolyte (>5 eV), while TiO_2 is also an insulator in the region of potentials that are much more positive than its conduction band potential. In these cases, $z_2 = \infty$ in the model of Figure 4, and the equivalent circuit of the film reduces to a two-channel TL.[11−14] At the potential of the HOMO of Z907 dye, it will be possible to transfer charge from the conducting substrate to the dye (channel 1), obtaining surface conduction through this monolayer.[26] The potentials for charge injection to the molecular layer are indicated in Figure 3, and transport in this layer is observed in Figure 8, were the impedance plot may be modeled by a TL with $z_1 = r_1$ and $y_0 = q_0(j\omega)^{\gamma_0}$. The hole percolation in TiO_2 is a perfect realization of the model of Figure 5 because the impedance spectrum exhibits exact doubling of exponents at low and high frequency required by the TL model,[14] as discussed before in connection to Figure 5. The porous alumina electrode shows a slightly smaller slope at low frequency, mainly due to the contribution of ion diffusion in the electrolyte, which is more difficult in this structure due to the smaller size of the channels.

At negative bias potentials approaching the conduction band of TiO_2, it becomes a semiconductor with a transport resistance that varies exponentially with applied potential.[19,33] Therefore, in the upper channel in Figure 4 we have $z_2 = r_2$. Furthermore, the surface-derivatized Z907 molecule monolayer is insulating when the potential is between the HOMO and LUMO levels[26] of Z907 as indicated in Figure 3, suggesting that electrons are merely moving through TiO_2 rather than through Z907 ($R_2 \ll R_1$).

At −0.4 V, the impedance plot shown in Figure 9 yields a plot similar to the simulation in Figure 6b. Alhough according to the model, it would correspond to a situation in which $R_2 < R_3$, the potential applied and the band positions shown in Figure 3 suggest that this possibility is unlikely. The effect at high frequency may be the result of the contribution of the back layer FTO/electrolyte capacitor that modifies the shape of the diffusive behavior of electrons through TiO_2.[33]

With decreasing potential, R_2 decreases rapidly and the diffusion pattern of impedance disappears from the plots, as indicated in Figure 9. Only a small and constant distortion can be seen in the intermediate frequency region that may be related to FTO/electrolyte or even FTO/TiO_2 interfaces. In the overall impedance, this effect is negligible in comparison with the low-frequency capacitive behavior, which shows an almost vertical straight line corresponding to the charging/discharging of the chemical capacitance of TiO_2.[3]

This brief analysis shows that the three-channel TL model makes it possible to determine the separate conductivity of semiconductor and organic phases, and interfacial charge transfer, in the functionalized nanostructured electrodes, depending on biasing conditions. A more detailed characterization will be presented in future work.

Acknowledgment. This work was supported by MCyT under project MAT2004-05168 and the Swiss National Science Foundation under the special NP-47 National program. We thank Dr. Shaik M. Zakeeruddin for providing the Z907 molecule and Mr. P. Comte for the mesoscopic metal oxide films.

References and Notes

(1) Bisquert, J. *J. Phys. Chem. B* **2002**, *106*, 325.
(2) Jamnik, J.; Maier, J. *Phys. Chem. Chem. Phys.* **2001**, *3*, 1668.
(3) Bisquert, J. *Phys. Chem. Chem. Phys.* **2003**, *5*, 5360.
(4) Pitarch, A.; Garcia-Belmonte, G.; Mora-Seró, I.; Bisquert, J. *Phys. Chem. Chem. Phys.* **2004**, *6*, 2983.
(5) Buck, R. P.; Mundt, C. *Electrochim. Acta* **1999**, *44*, 1999.
(6) Sah, C.-T. *Proc. IEEE* **1967**, *55*, 654.
(7) Sah, C.-T. *Proc. IEEE* **1967**, *55*, 672.
(8) Sah, C.-T. *Solid-State Electron.* **1970**, *13*, 1547.
(9) Paasch, G. *Electrochem. Commun.* **2000**, *2*, 371.
(10) Paasch, G. *Electrochim. Acta* **2002**, *47*, 2049.
(11) de Levie, R. In *Advances in Electrochemistry and Electrochemical Engineering*; Delahay, P., Ed.; Interscience: New York, 1967; Vol. 6; p 329.
(12) Paasch, G.; Micka, K.; Gersdorf, P. *Electrochim. Acta* **1993**, *38*, 2653.
(13) Lasia, A. *J. Electroanal. Chem.* **1995**, *397*, 27.
(14) Bisquert, J.; Garcia-Belmonte, G.; Fabregat-Santiago, F.; Ferriols, N. S.; Bogdanoff, P.; Pereira, E. C. *J. Phys. Chem. B* **2000**, *104*, 2287.
(15) Raistrick, I. D. *Electrochim. Acta* **1990**, *35*, 1579.
(16) Garcia-Belmonte, G.; Bisquert, J.; Pereira, E. C.; Fabregat-Santiago, F. *J. Electroanal. Chem.* **2001**, *508*, 48.
(17) Grätzel, M. *Nature* **2001**, *414*, 338.
(18) Cinnsealach, R.; Boschloo, G.; Rao, S. N.; Fitzmaurice, D. *Sol. Energy Mater. Sol. Cells* **1998**, *55*, 215.
(19) Fabregat-Santiago, F.; Bisquert, J.; Garcia-Belmonte, G.; Boschloo, G.; Hagfeldt, A. *Sol. Energy Mater. Sol. Cells* **2005**, *87*, 117.
(20) Kern, R.; Sastrawan, R.; Ferber, J.; Stangl, R.; Luther, J. *Electrochim. Acta* **2002**, *47*, 4213.
(21) Wang, Q.; Moser, J.-E.; Grätzel, M. *J. Phys. Chem. B* **2005**, *109*, 14945.
(22) Hoshikawa, T.; Kikuchi, R.; Eguchi, K. *J. Electroanal. Chem.* **2006**, *588*, 59.
(23) García-Cañadas, J.; Fabregat-Santiago, F.; Kapla, J.; Bisquert, J.; Garcia-Belmonte, G.; Mora-Seró, I.; Edwards, M. O. M. *Electrochim. Acta* **2004**, *49*, 745.
(24) Bonhôte, P.; Gogniac, E.; Sophie, T.; Barbé, C.; Vlachopoulos, N.; Lenzmann, F.; Comte, P.; Grätzel, M. *J. Phys. Chem. B* **1998**, *102*, 1498.
(25) Wang, Q.; Zakeeruddin, S. M.; Cremer, J.; Bäuerle, P.; Humphry-Baker, R.; Grätzel, M. *J. Am. Chem. Soc.* **2005**, *127*, 5706.
(26) Wang, Q.; Zakeeruddin, S. M.; Nazeeruddin, M. K.; Humphry-Baker, R.; Grätzel, M. *J. Am. Chem. Soc.* **2006**, *128*, 4446.
(27) Trammell, S. A.; Meyer, T. J. *J. Phys. Chem. B* **1999**, *103*, 104.
(28) Westermark, K.; Tingry, S.; Persson, P.; Rensmo, H.; Lunell, S.; Hagfeldt, A.; Siegbahn, H. *J. Phys. Chem. B* **2001**, *105*, 7182.
(29) Bisquert, J.; Garcia-Belmonte, G.; Fabregat-Santiago, F.; Compte, A. *Electrochem. Commun.* **1999**, *1*, 429.
(30) Brioullin, L. *Wave Propagation in Periodic Structures*; Dover: New York, 1953.
(31) Pajkossy, T. *J. Electroanal. Chem.* **1994**, *364*, 111.
(32) Pajkossy, T.; Wandlowski, T.; Kolb, D. M. J. *J. Electroanal. Chem.* **1996**, *414*, 209.
(33) Fabregat-Santiago, F.; Garcia-Belmonte, G.; Bisquert, J.; Zaban, A.; Salvador, P. *J. Phys. Chem. B* **2002**, *106*, 334.